Up-conversion properties of Yb,Tb:YAG single crystals grown by the micro-pulling-down method

Jian Liu, Qingsong Song, Jie Xu, Jun Guo, Yuxin Pan, Na Li, Dongzhen Li, Peng Liu, Xiaodong Xu, Jun Xu, et al.

Up-conversion properties of Yb,Tb:YAG single crystals grown by the micro-pulling-down method

Jian Liu[a], Qingsong Song[a], Jie Xu[b], Jun Guo[b], Yuxin Pan[c], Na Li[d], Dongzhen Li[b], Peng Liu[b], Xiaodong Xu[b,*], Jun Xu[a,*] Kheirreddine Lebbou[e,*]

[a] School of Physics Science and Engineering, Institute for Advanced Study, Tongji University, Shanghai 200092, China
[b] Jiangsu Key Laboratory of Advanced Laser Materials and Devices, School of Physics and Electronic Engineering, Jiangsu Normal University, Xuzhou 221116, China
[c] Engineering Research Center of Optical Instrument and System, Ministry of Education and Shanghai Key Lab of Modern Optics and Systems, University of Shanghai for Science and Technology, Shanghai, 200093, China
[d] School of Mathematics and Physics, Jinzhong University, Jinzhong 030619, PR China
[e] Institut Lumière Matière, UMR5306 UniversitéLyon1-CNRS, Université de Lyon, Lyon 69622, Villeurbanne Cedex, France

Corresponding author:
Email address: xdxu79@jsnu.edu.cn (X. Xu), xujun@mail.shcnc.ac.cn (J. Xu)
Kheirreddine.lebbou@univ-lyon1.fr (K. Lebbou)

Abstract: Yb,Tb:YAG crystals with various Yb^{3+} and Tb^{3+} concentration were grown by the micro-pulling-down technique (μ-PD). The absorption spectra, fluorescence spectra and fluorescence decay curves of Yb,Tb:YAG crystals were measured at room temperature. Under 980 nm excitation, Yb,Tb:YAG crystals exhibited intense visible up-conversion luminescence due to the cooperative energy transfer from two Yb^{3+} ions to one Tb^{3+} ion. Under 4850 nm excitation, Yb,Tb:YAG crystals yielded near-infrared down-conversion emission, ascribing to the cooperative absorption of pumping photons and cooperative energy transfer from one Tb^{3+} ion to two Yb^{3+} ions. The energy transfer processes from Yb^{3+} ions to Tb^{3+} ions were discussed, and the energy transfer efficiency was calculated. The results show that Yb,Tb:YAG crystal is promising for visible laser output when pumped by InGaAs laser diode (LD).

Keywords: Up-conversion; Micro-pulling-down technique; Visible laser; Energy transfer

1. Introduction

Nowadays, much attention has been paid to rare-earth doped materials for their visible emission, which can be used in iatrology, biomedical diagnosis, astronomy and telecommunication [1-4]. Tb^{3+}-doped materials could emit the sharp and intense fluorescence in the yellow-green range, which are considered to be promising materials for practical use. Especially, the yellow emission around 587 nm matches well with the D2 absorption line of sodium atoms, which can be used to excite the sodium layer at attitude of ~ 90 km in the laser guide system [5-9]. Unfortunately, the relevant pumping source around 485 nm is immature, the price of the pumping device is expensive. Normally, the pump radiation was offered by a frequency-doubled optically pumped semiconductor laser (2ω-OPSL) [10-15].

In the Yb^{3+}/Tb^{3+} co-doped system, Yb^{3+} ions are used as sensitizer ions. Yb^{3+} ion was considered as a sensitized ion since 1960s for its large absorption cross section, and was widely used with commercially application of the 976 LD pump sources. Up-conversion is an anti-Stokes process to convert near infrared light to visible light. A lot of efforts have been focused on the fluoride materials doped with different rare earth ions, such as Ho^{3+}, Tm^{3+} and Er^{3+} as activators and Yb^{3+} ions as sensitizers [15-17]. For the reason that the low phonon energy of the fluorides is beneficial for the high up-conversion efficiency achievement. However, fluorides exhibit relatively poor stability, and in comparison, YAG single crystal is an excellent laser gain medium due to its high thermal conductivity and excellent physical and chemical properties [18], which play a crucial role in practical application. Compared with Yb^{3+}/Ho^{3+}, Yb^{3+}/Tm^{3+}, Yb^{3+}/Er^{3+} co-doped materials, the energy transfer in Yb^{3+}/Tb^{3+} co-doped materials are different. There do not exist immediate level available for the energy transfer. For the Yb^{3+}/Tb^{3+} dopants, the mechanism of up-conversion is called cooperative energy transfer (CET), two excited Yb^{3+} (sensitizer) ions simultaneously transfer their energy to one Tb^{3+} (activator) ion, and the Tb^{3+} is excited to the $^5D4$ level. In previous literatures, some works had been done in Yb^{3+}/Tb^{3+} co-doped materials [19-22]. However, Yb^{3+}/Tb^{3+} co-doped YAG crystal has never been reported. It is necessary to explore the potential of Tb^{3+} ions in YAG crystal for visible laser output through up-conversion process.

The micro-pulling-down (μ-PD) technique allows the growth of fiber-shaped single crystals with high pulling rate. It has many advantages over the conventional crystal growth techniques, such as controllable crystal shape and low cost that includes raw materials and time saving. The crystals grown by the μ-PD technique showed good laser performance [23-27].

In this paper, Yb^{3+}/Tb^{3+} co-doped YAG single crystals were grown by the μ-PD technique. We mainly report the cooperative sensitized up-conversion of the Yb^{3+}/Tb^{3+} co-doped YAG single crystals. The spectroscopic properties including the absorption spectra, fluorescence spectra, fluorescence decay curves were studied.

2. Experimental

The Yb,Tb:YAG single crystals were grown by the μ-PD method. The high purity powders Tb_4O_7 (99.99%), Yb_2O_3 (99.999%), Al_2O_3 (99.999%), Y_2O_3 (99.999%) were used as raw materials and weighed according to the formula $(Y_{1-x-y}Tb_xYb_y)_3Al_5O_{12}$ (x=0-0.16; y=0-0.16). The powders were pressed into bulks and sintered at 1300 °C for 20 h in the air. Then the polycrystalline materials were loaded into an iridium crucible for crystal growth. The

experimental model of the micro-pulling-down technique (μ-PD) is described as Figure.1. The <111> oriented pure YAG crystal was used as the seed and pulled down continuously with a pulling rate 0.3 mm/min. The molten zone, the meniscus and part of the grown crystal were directly observed and monitored with a CCD camera through the insulating hole. The detail of the crucible part was shown in Figure. 1 (b). The Yb:Tb codoped YAG melts wet well the lip of the crucible, it is fixed at the bottom of the capillary die. Adjustment of fiber diameter was realized by controlling the RF power supply and the pulling rate. Increase of the crucible temperature and pulling rate results in decrease of the fiber diameter. The higher RF power will be accompanied by larger thickness of the melt film between the crucible and the fiber. The as-grown crystals were shown in Fig. 2(a). The crystals are transparent with green color, which was due to the oxygen vacancies and formed Re-F color center in Yb,Tb:YAG crystals [28]. After annealed in the air for 12 hours at 1250 °C, the crystals changed from green to colorless, as shown in Fig. 2(b).

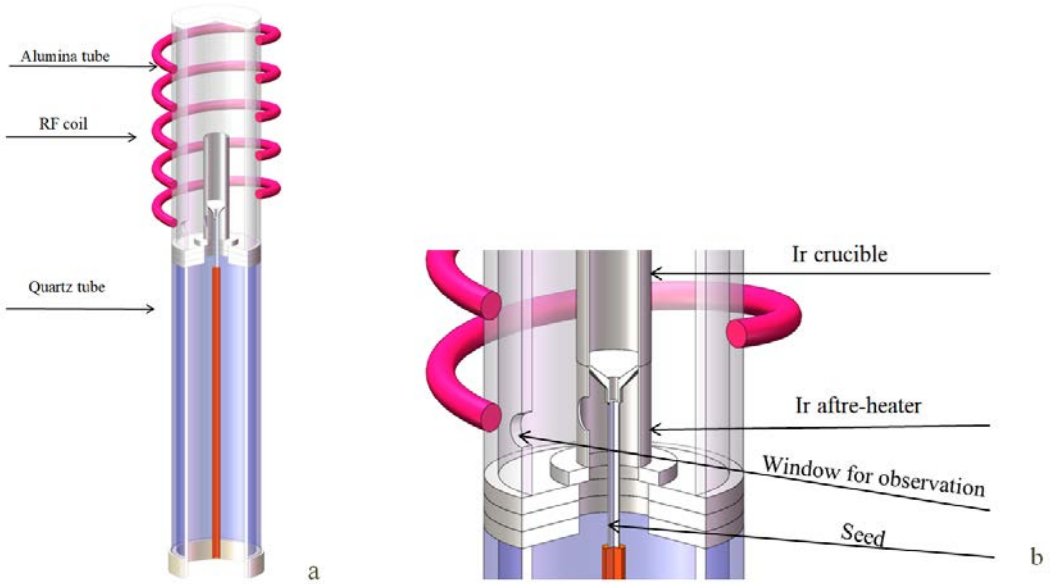

Figure 1. Schematic illustration of the micro-pulling-down technique.

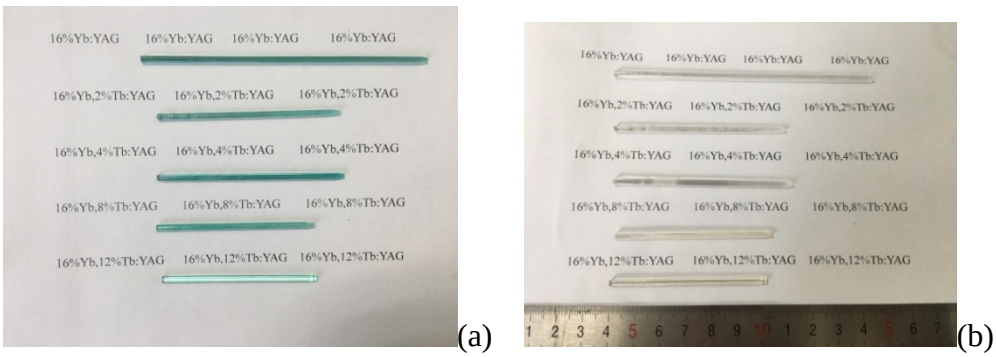

Figure 2. Photographs of (a) as-grown Yb,Tb:YAG crystals and (b) after annealing in the air.

Powders crushed from the grown crystal was used to determine the crystal structure. The phase compositions of all the samples were characterized using an X-ray diffraction (XRD) machine equipped with a copper target X-ray tube (D2 Avance, Bruker, Karlsruhe, Germany)

in the scanning range of 10°–90°. The morphology of the polished Yb,Tb:YAG crystals were recorded on a scanning electron microscope (SEM, JSM-6510, JEOL, Kariya, Japan). The absorption spectra of Yb,Tb:YAG crystals were measured using a spectrophotometer (Lambda 950, Perkin -Elmer UV–VIS–NIR) in the wavelength range of 300–3000 nm. The emission properties of the Yb,Tb:YAG crystals were recorded by an Edinburgh Fluorescence under 485 nm and 980 nm excitation. All the measurements were performed at room temperature.

3. Results and discussion

The XRD patterns of the as-grown Yb,Tb:YAG crystals for the different Yb^{3+} and Tb^{3+} concentrations, together with the standard pattern of pure YAG crystal, are shown in Fig. 3. As can be seen, the observed peaks fit well with the pure YAG phase, which indicates that the synthesized Yb,Tb:YAG crystals are isostructural with YAG crystal and the high concentration dopant did not cause any significant impact on the phase structure. Not any new secondary phase could be observed in the grown Yb, Tb codoped yttrium aluminium garnet. The lattice parameters for the doped crystals were calculated using the JADE software. The lattice constants of Yb,Tb:YAG crystals were calculated to be 1.1919, 1.1954, 1.1977, 1.1995 and 1.2001 nm for the $Yb_{0.16}$, $Yb_{0.16}Tb_{0.02}$, $Yb_{0.16}Tb_{0.04}$, $Yb_{0.16}Tb_{0.08}$ and $Yb_{0.16}Tb_{0.12}$ crystals, respectively. The lattice parameters were smaller than that of YAG crystal (1.2008 nm). As it can be seen, the size of the unit cell monotonously increases as Tb^{3+}-doping concentration level increases. This expansion of the unit cell can be attributed to the larger radius of Tb^{3+} ions.

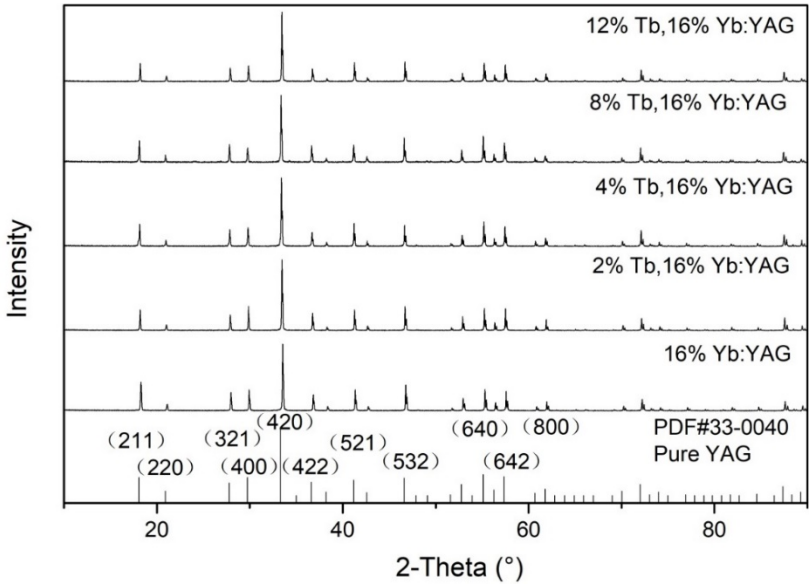

Figure 3. Room temperature XRD spectra of Yb,Tb:YAG crystals with different dopants concentration.

The room temperature absorption spectra of Yb,Tb:YAG crystals in the range of 300-2500 nm were shown in Fig. 4. The observed absorption bands are assigned to the transitions from the ground states of Tb^{3+}:$^7F_6$ or Yb^{3+}:$^2F_{7/2}$ to the excited ones. Because of the low Tb concentration, the absorptions are intense and narrower, it is related to the ions which are located in more defined coordination sites within the garnet structure. As shown in the inset of

Fig 4(a), the weak band at 486 nm related to the $^7F_6 \rightarrow {}^5D_4$ transition of Tb^{3+}, which matches well with the emission wavelength of frequency-doubled optically pumped semiconductor laser, is usually used for pumping of Tb^{3+} laser. The absorption coefficient at 486 nm was calculated to be 0.04, 0.08, 0.17 and 0.21 cm^{-1} for the $Yb_{0.16}Tb_{0.02}$, $Yb_{0.16}Tb_{0.04}$, $Yb_{0.16}Tb_{0.08}$ and $Yb_{0.16}Tb_{0.12}$ crystals, respectively. The intense absorption in the 850-1050 nm wavelength region is due to the absorption of Yb^{3+} ions, which is attributed to the $^2F_{7/2} \rightarrow {}^2F_{5/2}$ transition. As the Yb^{3+} doping concentration increases from 2 at.% to 16 at.% with the same Tb^{3+} doping concentration of 8 at.%, the absorption coefficient at 940 nm increases linearly from 2.0 cm^{-1} to 16.1 cm^{-1} as shown in the inset of Fig. 4(b).

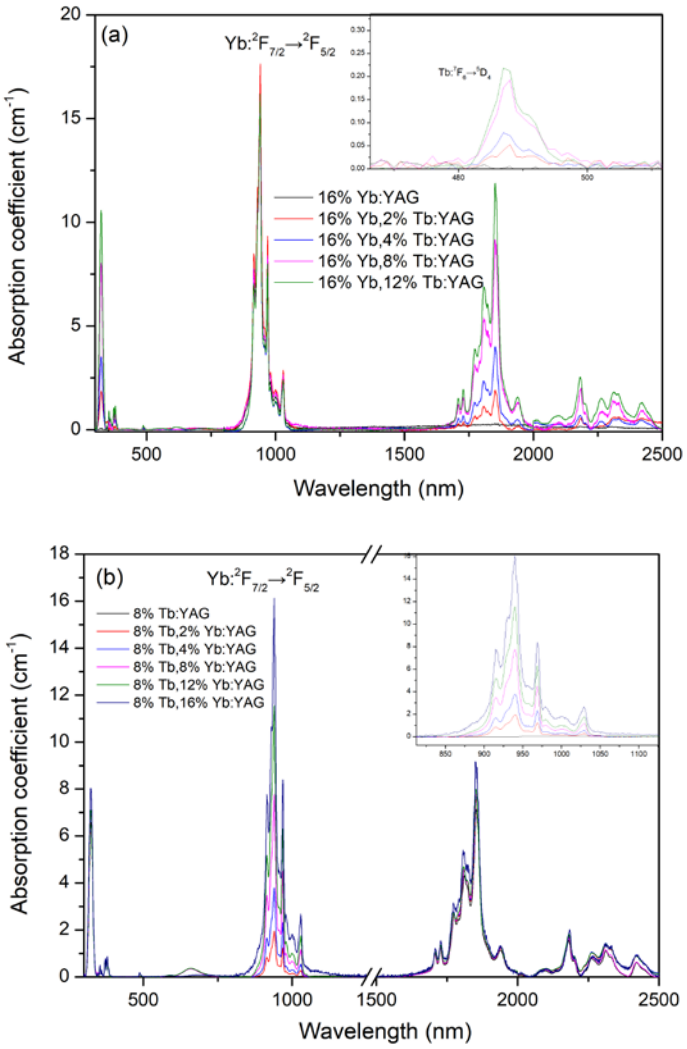

Figure 4. Room temperature absorption spectra of Yb,Tb:YAG crystals
(a) $Yb_{0.16}Tb_x$ (x=0, 0.02, 0.04, 0.08, 0.12):YAG crystals
(b) $Yb_yTb_{0.08}$ (y=0.02, 0.04, 0.08, 0.12, 0.16):YAG crystals.

Fig. 5 displays the up-conversion spectra of the Yb,Tb:YAG crystals under 980 nm excitation at room temperature. Most of the typical emission lines from the f-f transitions of Yb^{3+} and Tb^{3+}, can be detected. The Yb,Tb:YAG crystals exhibit intense visible luminescence and three distinguished bands are corresponding to the transitions from $^5D_4$ energy level to $^7F_5$, $^7F_4$ and $^7F_3$ energy levels of Tb^{3+} ions, respectively. The characteristic positions of the

emission peaks were nearly the same among the nine Yb,Tb:YAG samples. The emission spectra of Tb^{3+} at different concentration are shown in Fig. 5(a). For comparison, we did not register the emission of Yb:YAG crystal within the test wavelength range. When the concentration of Tb^{3+} 8 at.%, the emission intensity of $^5D_4$ reaches the maximum. In order to investigate the energy transfer from Yb^{3+} to Tb^{3+}, we grew a series of Yb,Tb:YAG crystals with different Yb^{3+} concentration. Fig. 5(b) presents the emission spectra of Tb^{3+} with different Yb^{3+} concentration. The trend in the variation of the up-conversion intensity at 543 nm, 587 nm and 623 nm due to the influence of the Yb^{3+} concentration is shown in the inset of Fig. 5(b). The emission intensity increases gradually with the increase of Yb^{3+} concentration from 2 at.% to 8 at.%, because the distance between Yb^{3+} and Tb^{3+} ions is shortened by the increasing concentration of Yb^{3+}, which inducing the improved energy transfer efficiency between rare earth ions and enhanced emission intensity. Then the emission intensity decreases with the further increase of the concentration of Yb^{3+}, which is due to quenching effect resulting from the pairing or aggregation of Yb^{3+} ions [22].

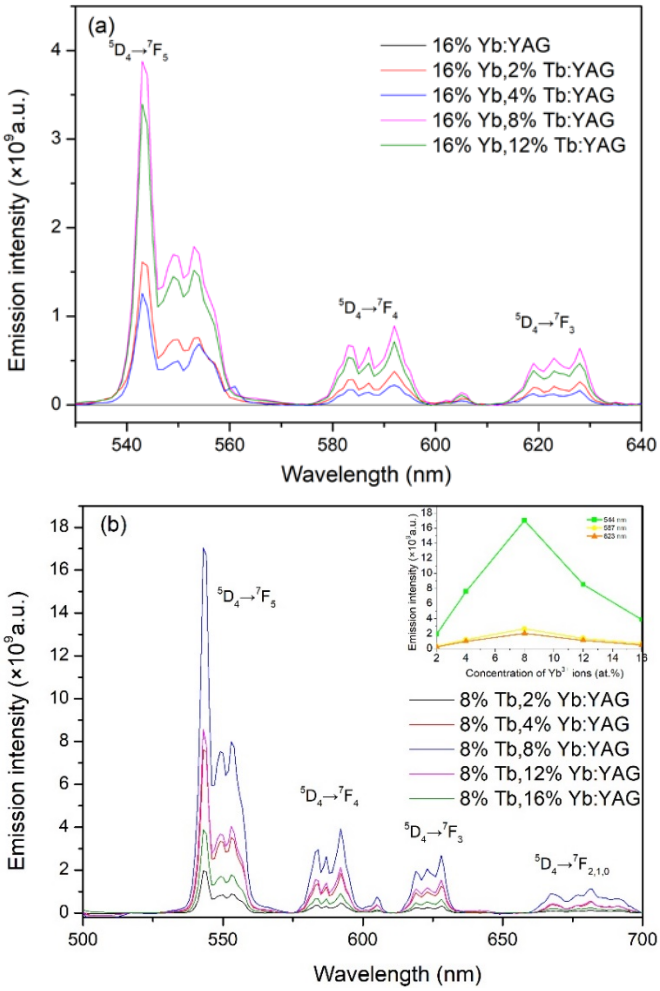

Figure 5. Room temperature emission spectra of Yb,Tb:YAG crystals excited at 980 nm
(a) $Yb_{0.16}Tb_x$ (x=0, 0.02, 0.04, 0.08, 0.12):YAG crystals
(b) $Yb_yTb_{0.08}$ (y=0.02, 0.04, 0.08, 0.12, 0.16):YAG crystals.

Fig. 6 illustrates the simplified energy levels of Yb^{3+} and Tb^{3+} in Yb,Tb:YAG crystal and

the up-conversion mechanisms under 980 nm excitation are indicated. The difference in the energy transfer efficiencies between Tb^{3+} and Yb^{3+} in YAG can be explained by the nature of the transitions in Tb^{3+} and Yb^{3+} ions. Pumping at 980 nm, the Yb^{3+} ions are excited from ground state $^2F_{7/2}$ to the excited state $^2F_{7/2}$, then efficient cooperative sensitization takes place easily from two Yb^{3+} ions to their neighbor Tb^{3+} ion, and the excited state $^5D_4$ of Tb^{3+} is populated largely. The cooperative energy transfer can be described as follows: Yb^{3+}:$^2F_{5/2}$ + Yb^{3+}:$^2F_{5/2}$ + Tb^{3+}:$^7F_6$ → Yb^{3+}:$^2F_{7/2}$ + Yb^{3+}:$^2F_{7/2}$ + Tb^{3+}:$^5D_4$. The cooperative energy transfer process produce the 543 nm, 587 nm and 623 nm emission originated from $^5D_4$ → ^7F_J (J= 5, 4, 3) transitions.

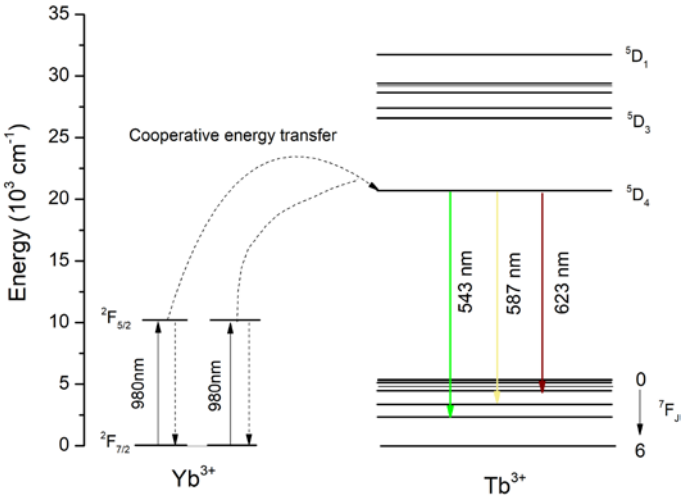

Figure 6. Simplified energy levels of Yb^{3+} and Tb^{3+} in Yb,Tb:YAG crystal and transition mechanisms

The room temperature emission spectra of Yb,Tb:YAG crystals excited by 485 nm were also recorded, as shown in Fig. 7. The visible emission intensity increases gradually with the increase of Tb^{3+} concentration, indicating that no concentration quenching occurs even the Tb^{3+} concentration is as high as 12 at.%. The characteristic emission bands located at 900-1100 nm due to the $^2F_{5/2}$ → $^2F_{7/2}$ transition of Yb^{3+} are observed for both Yb^{3+} singly doped and Yb^{3+}, Tb^{3+} doped YAG crystals. The two Yb^{3+} ions were exited together from the ground state $^2F_{7/2}$ to the excited state $^2F_{5/2}$ by means of cooperative absorption of pumping photons and or/ by cooperative energy transfer process from $^5D_4$ level of Tb^{3+} to Yb^{3+}: Tb^{3+}:$^5D_4$ + Yb^{3+}:$^2F_{7/2}$ + Yb^{3+}:$^2F_{7/2}$ → Tb^{3+}:$^7F_6$ + Yb^{3+}:$^2F_{5/2}$ + Yb^{3+}:$^2F_{5/2}$ [29]. The cooperative absorption process is dominant to the excitation of Yb^{3+}:$^2F_{5/2}$ level by cooperative absorption because Yb^{3+} has a much large absorption coefficient around 970 nm than Er^{3+} around 485 nm. When the concentration of Tb^{3+} increased to 12 at.%, the emission intensity at 1029 nm reached the maximum, showing the effective cooperative down-conversion process from one Tb^{3+} ion to two Yb^{3+} ions.

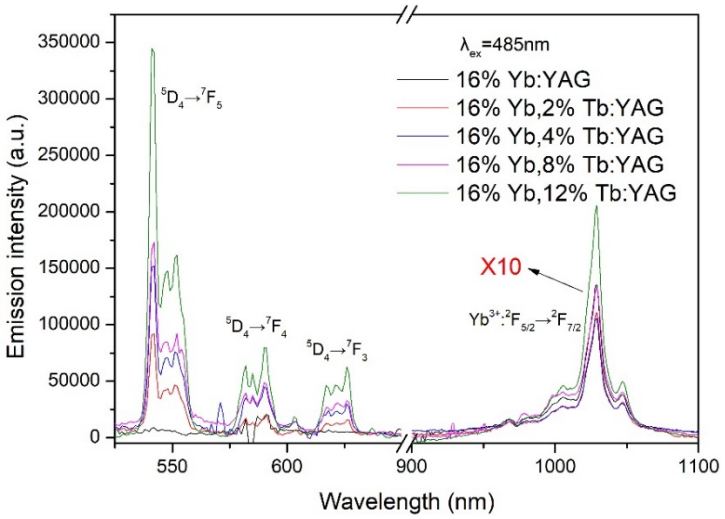

Figure 7. Room temperature emission spectra of $Yb_{0.16}Tb_x$ (x=0, 0.02, 0.04, 0.08, 0.12):YAG crystals excited at 485 nm

The fluorescence decay curves corresponding to the $^2F_{5/2} \rightarrow {}^2F_{7/2}$ transition are shown in Fig. 8, which were monitored at 1050 nm and excited at 980 nm. The fluorescence lifetime for the $^2F_{5/2}$ multiplet were estimated and listed in Table 1. Owing to radiative trapping [30], the measured fluorescence lifetime of Yb:YAG crystal is longer than the intrinsic fluorescence lifetime (0.951 ms). The decay lifetime decreases with the increasing of Tb^{3+} content, which can be explained by the cooperative energy transfer from Yb^{3+}:$^2F_{5/2}$ to Tb^{3+}:$^5D_4$.

The cooperative energy transfer efficiency from Yb^{3+} to Tb^{3+} in Yb,Tb:YAG crystals can be calculated by using the formula $\eta_{ET}=1-\tau_x/\tau_0$ [31]. Where τ_0 is the fluorescence lifetime of the singly Yb^{3+} doped YAG crystal, τ_x stands for the fluorescence lifetime of Yb^{3+} ions in the presence of Tb^{3+} ions. As listed in Table 1, the energy transfer efficiency from Yb^{3+} to Tb^{3+} ions was calculated to be 3.4%, 16.3%, 27.8%, and 45.4% for the $Tb_{0.02}Yb_{0.16}$, $Tb_{0.04}Yb_{0.16}$, $Tb_{0.08}Yb_{0.16}$, and $Tb_{0.12}Yb_{0.16}$ samples, respectively. All the results show that Yb,Tb:YAG crystal could be a promising visible laser medium when pumped by InGaAs laser diode (LD).

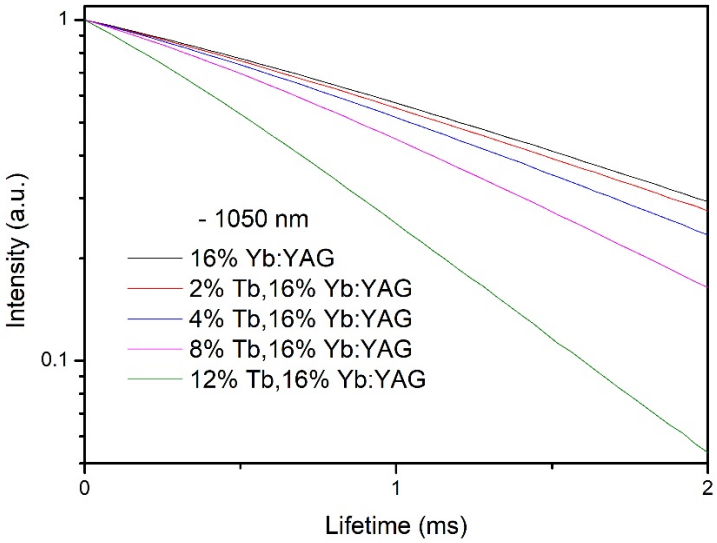

Figure 8. Decay curves of $^2F_{5/2}$ multiplet of Yb,Tb:YAG crystals under excitation of 980 nm.

Table 1. Measured lifetime of $^2F_{7/2}$ multiplet of Yb^{3+} and cooperative energy transfer efficiency from Yb^{3+} to Tb^{3+} in $Yb_{0.16}Tb_x$:YAG x=(0, 0.02, 0.04, 0.08, 0.12) crystals

$Yb_{0.16}Tb_x$:YAG	τ_{Yb} (ms)	η_{ET} (%)
0	1.61	-
0.02	1.55	3.4
0.04	1.34	16.3
0.08	1.15	27.8
0.12	0.87	45.4

4. Conclusion:

Tb^{3+} and Yb^{3+} co-doped YAG single crystals were grown using the micro-pulling-down method. The room temperature XRD showed that the high concentration dopant did not change the garnet phase structure and do not provide impurities. The effect of Yb^{3+} and Tb^{3+} concentration on absorption spectra, emission spectra and fluorescence lifetimes of Yb,Tb:YAG crystals were investigated at room temperature. The absorption coefficient showed the concentration dependence. Under 980 nm excitation, Yb,Tb:YAG crystals exhibited intense visible up-conversion luminescence due to the cooperative energy transfer from two Yb^{3+} ions to one Tb^{3+} ion. The cooperative energy transfer mechanism between Yb^{3+} and Tb^{3+} ions was discussed and the energy transfer efficiency was calculated. Moreover, the cooperative down-conversion process from one Tb^{3+} ion to two Yb^{3+} ions was also studied. The results show that Yb,Tb:YAG crystal is promising for visible laser output when pumped by InGaAs laser diode (LD).

Acknowledgements

This work is partially supported by National Natural Science Foundation of China (No.61805177 and No. 61621001), Fund of Key Laboratory of Optoelectronic Materials Chemistry and Physics, Chinese Academy of Sciences (No. 2008DP173016), MOE Key Laboratory of Advanced Micro-Structured Materials, “Qinglan Project” of the Young and Middle-aged Academic Leader of Jiangsu College and University.

References:

[1] C. Kränkel, D. T. Marzahl, F. Moglia, G. Huber, P.W. Metz, Out of the blue: semiconductor laser pumped visible rare-earth doped lasers, Laser Photonics Rev. 10 (2016) 1-21.

[2] M. A. Mainster, Wavelength Selection in Macular Photocoagulation: Tissue Optics, Thermal Effects, and Laser Systems, Ophthalmology 93 (1986) 952-958.

[3] M. Duering, V. Kolev, and B. Luther-Davies, Generation of tunable 589 nm radiation as a Na guide star source using an optical parametric amplifier, Opt. Express 17 (2009) 437-446.

[4] P. Juncar, J. Pinard, J. Hamon, and A. Chartier, Absolute Determination of the Wavelengths of the Sodium D1 and D2 Lines by Using a CW Tunable Dye Laser Stabilized on Iodine, Metrologia 17 (1981) 77.

[5] C. E. Max, S. S. Olivier, H. W. Friedman, J. An, K. Avicola, B. V. Beeman, H. D. Bissinger, J. M. Brase, G. V. Erbert, D. T. Gavel, K. Kanz, M. C. Liu, B. Macintosh, K. P. Neeb, J. Patience, K. E. Waltjen, Image improvement from a sodium-layer laser guide star adaptive optics system, Science 277 (1997) 4.

[7] J. W. Beletic, Designer detectors: a new paradigm for instrument development, Proc.SPIE 5382 (2004) 706-717.

[8] L. Zhang, H. Jiang, S. Cui, J. Hu, Y. Feng, Versatile Raman fiber laser for sodium laser guide star, Laser Photonics Rev. 8 (2015) 889-895.

[9] K. Wei, M. Li, S.Q. Chen, Y. Bo, F. Chen, J.W. Zuo, Q. Bian, J. Yao, L.C. Zhou, L. Wei, First light for the sodium laser guide star adaptive optics system on the Lijiang 1.8m telescope, Res. Astron. Astrophys. 16 (2016) 41-45.

[10] P. W. Metz, C. Kränkel, G. Huber, Efficient green and yellow lasers in Tb^{3+}-doped $LiYF_4$, $LiLuF_4$, and KY_3F_{10} crystals, EPS-QEOD Europhoton Conference FrB-T1-O-07, Neuchâtel, Switzerland 2014.

[11] P. W. Metz, D. T. Marzahl, A. Majid, C. Kränkel, G. Huber, Efficient continuous wave laser operation of Tb^{3+}-doped fluoride crystals in the green and yellow spectral regions, Laser Photonics Rev. 10 (2016) 335-544.

[12] P. W. Metz, D. T. Marzahl, G. Huber, C. Kränkel, Performance and wavelength tuning of green emitting terbium lasers, Opt. Express 25 (2017) 5716-5724.

[13] E. C. Hernández, P. W. Metz, M. Demesh, and C. Kränkel, Efficient directly emitting high-power Tb^{3+}:$LiLuF_4$ laser operating at 587.5 nm in the yellow range, Opt. Lett. 43 (2018) 4791-4794.

[14] H. Chen, H. Uehara, H. Kawase and R. Yasuhara, Efficient visible laser operation of Tb:$LiYF_4$ and $LiTbF_4$, Opt. Express 28 (2020) 10951-10959.

[15] H. Chen, W. Yao, H. Uehara, and R. Yasuhara, Graphene Q-switched Tb:$LiYF_4$ green laser, Opt. Lett. 45 (2020) 2596-2599.

[15] A. Pilch, D. Wawrzyńczyk, M. Kurnatowska, B. Czaban, M. Samoć, W. Strek, A. Bednarkiewicz, The concentration dependent up-conversion luminescence of Ho^{3+} and Yb^{3+} co-doped b-$NaYF_4$, J. Lumin. 182 (2017) 114 -122.

[16]L. M. Jin, X. Chen, C. K. Siu, F. Wang, S. F. Yu, Enhancing multiphoton upconversion from $NaYF_4$: Yb/Tm@NaYF4 core-shell nanoparticles via the use of laser cavity, ACS Nano (2017) 843-849.

[17] M. K. Gnanasammandhan, N. M. Idris, A. Bansal, K. Huang, Y. Zhang, Near-IR

photoactivation using mesoporous silica-coated NaYF4: Yb, Er/Tm upconversion nanoparticles, Nat. Protoc. 11 (2016) 688-713.
[18] X. Xu, Z. Zhao, P. Song, J. Xu, P. Deng, Structural, thermal and luminescent properties of Yb-doped $Y_3Al_5O_{12}$ crystals, J. Opt. Soc. Am. B. 21 (2004) 543-547
[19] Y. Arai, T. Yamashidta, T. Suzuki, and Y. Ohishi, Upconversion properties of Tb^{3+}-Yb^{3+} codoped fluorophosphates glasses, J. Appl. Phys. 105 (2009) 083105
[20] X. S. Qiao, X. P. Fan, Z. Xue, X. H. Xu, Q. Luo, Intense ultraviolet upconversion luminescence of Yb^{3+} and Tb^{3+} co-doped glass ceramics containing SrF_2 nanocrystals, J. Lumin. 131 (2011) 2036-2041.
[21] T. Grzy, K. Kubasiewicz, A. Szczeszak, S. Lis, Energy migration in YBO_3:Yb^{3+},Tb^{3+} materials: Down- and upconversion luminescence studies, J. Alloy Compd. 686 (2016) 951-961.
[22] H. N. Huang, T. Wang, H. F. Zhou, D. P. Huang, Y. Q. Wu, G. J. Zhou, J. F. Hu, J. Zhan, Luminescence, energy transfer, and up-conversion mechanisms of Yb^{3+} and Tb^{3+} co-doped $LaNbO_4$, J. Alloy Compd. 702 (2017) 209-215.
[23] J. L. Wang, Q. S. Song, Y. W. Sun, Y. G. Zhao, W. Zhou, D. Z. Li, X. D. Xu, C. F. Shen, W. C. Yao, L. Wang, J. Xu, D. Y. Shen, High-performance Ho:YAG single-crystal fiber laser in-band pumped by a Tm-doped all-fiber laser, Opt. Lett. 44 (2019) 455-458.
[24] Y. Y. Xue, N. Li, Q. S. Song, X. D. Xu, X. T. Yang, T. Y. Dai, D. H. Wang, Q. G. Wang, D. Z. Li, Z. S. Wang, J. Xu, Spectral properties and laser performance of Ho:CNGG crystals grown by the micro-pulling-down method, Opt. Mater. Express 9 (2019) 2490-2496.
[25] Y. G. Zhao, L. Wang, W. D. Chen, J. L. Wang, Q. S. Song, X. D. Xu, Y. Liu, D. Y. Shen, J. Xu, X. Mateos, P. Loiko, Z. P. Wang, X. G. Xu, U. Griebner, and V. Petrov, 35 W continuous-wave Ho:YAG single-crystal fiber laser, High Power Laser Science and Engineering, 8 (2020) e25.
[26] Y. Y. Xue, N. Li, D. H. Wang, Q. G. Wang, B. Liu, Q. S. Song, D. Z. Li, X. D. Xu, Z. P.Qin, Z. S. Wang, J. Xu, Spectroscopic and laser properties of Tm:CNGG crystals grown by the micro-pulling-down method, J. Lumin. 213 (2019) 36-39.
[27] Y.Q. Cai, B. Xu, Y. S. Zhang, Q. Y. Tian, X. D. Xu, Q. S. Song, D. Z. Li, J. Xu, I. Buchvarov, High power and energy generation in a Nd:YAG single-crystal fiber laser at 1834 nm, Photon. Res. 7 (2019) 162-166.
[28] J. Liu, Q. S. Song, D. Z. Li, Y. C. Ding, X. D. Xu, J. Xu, Spectroscopic properties of Tb:$Y_3Al_5O_{12}$ crystal for visible laser application, Opt. Mater. 106 (2020) 110001.
[29] X. Liu, S. Ye, Y. Qiao, G. Dong, B. Zhu, D. Chen, et al., Cooperative downconversion and near-infrared luminescence of Tb^{3+}-Yb^{3+} codoped lanthanum borogermanate glasses, Appl. Phys. B 96 (2009) 51-55
[30] D. S. Sumida and T. Y. Fan, Effect of radiation trapping on fluorescence lifetime and emission cross section measurements in solid-state media, Opt. Lett. 19 (1994) 1343-1345.
[31] S. Ye, B. Zhu, J.X. Chen, J. Luo, J.R. Qiu, Infrared quantum cutting in Tb^{3+},Yb^{3+} codoped transparent glass ceramics containing CaF_2 nanocrystals Appl. Phys. Lett. 92, (2008) 141112